

Millimeter line observations toward four local galaxies

Fei Li,^{1,2,3*} Junzhi Wang,^{1,4†} Minzhi Kong,^{3‡} Shanghuo Li,^{1,2,5}

¹Shanghai Astronomical Observatory, Chinese Academy of Sciences, 80 Nandan Road, Shanghai 200030, China

²University of Chinese Academy of Sciences, 19A Yuquanlu, Beijing 100049, China

³Hebei Normal University, No.20 Road East, 2nd Ring South, Yuhua District, Shijiazhuang, Hebei, 050024, China

⁴Key Laboratory of Radio Astronomy, Chinese Academy of Sciences, Nanjing, 210008, China

⁵Harvard-Smithsonian Center for Astrophysics, 60 Garden Street, Cambridge, MA 02138

Accepted XXX. Received YYY; in original form ZZZ

ABSTRACT

We present results of millimeter line observations toward four local gas-rich galaxies (NGC 3079, NGC 4258, NGC 6240 and VII Zw 31) with the IRAM 30 meter millimeter telescope. More than 33 lines in these four sources were detected, including normal dense gas tracers (HCN 1-0, HCO⁺ 1-0, and C₂H 1-0, etc) and their isotopic species. H¹³CN (1-0) and H¹³CO⁺ (1-0) are detected for the first time in NGC 4258. Optical depths of HCN 1-0 and HCO⁺ 1-0 were estimated with detected isotopic lines in NGC 4258, which were 4.1 and 2.6, respectively. HC₃N $J = 29 - 28$, which requires high volume density and high temperature to excite, was detected in NGC 6240. High ratios of HCO⁺/HCN in NGC 4258 and NGC 6240 imply that this ratio might not be a perfect diagnostic tool between AGN and starburst environments, due to contamination/combination of both processes. The low HC₃N/HCN line ratios with less than 0.15 in NGC 4258, NGC 6240 and the non-detection of HC₃N line in NGC 3079 and VII Zw 31 indicates that these four galaxies are HC₃N-poor galaxies. The variation of fractional abundance of CN in different types of galaxies is large.

Key words: galaxies:ISM– galaxies: individual: NGC 3079, NGC 4258, NGC 6240, VII Zw 31– galaxies: active

1 INTRODUCTION

Molecular interstellar medium (ISM) plays an essential role in star formation (Omont 2007), where star formation takes place (Solomon et al. 1979). Molecular gas is not only as fuel in the active process of galaxies but should also, in turn, be strongly affected by the activity (Krips et al. 2008). Molecular line observations, based on millimeter facilities, are crucial for understanding the physical and astro-chemical conditions of galaxies, which can provide plenty of information about density, mass, temperature, kinematics, magnetic field and so on (van Dishoeck & Blake 1998).

Multi-line studies of local galaxies have been made in literature (Walter et al. 2017; Martín et al. 2015; Davis et al. 2013; Aladro et al. 2013; Gao & Solomon 2004). Observational and theoretical works (Greve et al. 2009; Martín et al. 2009) showed that the thermal and astro-chemical structures of gas in nearby galaxies should differ between starburst (SB) and active galactic nucleus (AGN) dominated

regions. The activity in galaxy can be either an starburst or an AGN, or a combination of both. Gas properties derived from molecular lines can infer which physical process of activity dominates the heating of molecular cloud. Some studies had been done to distinguish between AGNs and starburst signatures of centers of galaxies (Kohno et al. 2001; Imanishi et al. 2004; Krips et al. 2008). Because the existence of both starburst and AGN can create exceptional and extreme conditions for the molecular gas in the central region, more spectral lines should be detected in AGN+SB composite galaxies than pure AGN-dominated galaxy. However, the connection between AGN and starburst are still not well understand. Local galaxies with both AGN and SB activities, are ideal targets for multiline studies of heavy rotor molecules.

In this paper, we present results of millimeter spectroscopy observations toward two nearby galaxies: NGC 3079, NGC 4258, and two Ultra-luminous infrared galaxies (ULIRGs): NGC 6240, VII Zw 31. The outline of this paper is as follows: we introduce the properties of the four sources in §2 the observations and data reduction in §3, and describe the main results of the data in §4. In §5, we present the anal-

* E-mail: lifei@shao.ac.cn

† E-mail: jzwang@shao.ac.cn

‡ E-mail: confucious_76@163.com

ysis and discussion of the results. And a brief summary is provided §6.

2 SOURCE SELECTION

We select four local galaxies to study molecular gas properties, with different nature of nuclear activities. NGC 3079 and NGC 4258 are two nearby type II AGN with strong H₂O maser emission, while NGC 6240 and VII Zw 31 are two gas-rich (U)LIRGs. Our original proposals were searching for SiO mega-masers in NGC 3079 and NGC 4258 at 3 mm band from about 85 GHz to 92 GHz, and searching for red-shifted 118.75 GHz molecular oxygen in NGC 6240 and VII Zw 31, which covers the rest frequencies from about 111 GHz to 119 GHz. NGC 3079, NGC 4258 and NGC 6240 are well studied and have relatively bright molecular emission lines.

NGC 3079, classified as a type II Seyfert galaxy (Sosa-Brito et al. 2001), is an edge-on spiral galaxy with optical and radio nuclear activity at the distance of 16.1 Mpc (Tsai & Hwang 2015). The central region not only hosts a AGN, but also hosts a powerful starburst. Dense gas tracers (CN, HCO⁺, and HNC 3-2 & 1-0 lines) of this source were reported by Pérez-Beaupuits et al. (2007), which concluded that emissions of HNC and HCN emerge from the same gas and the ratios of HCN/HNC and CN/HNC favor a PDR scenario, rather than an XDR. HCO⁺/HCN 1-0 line ratio is 1.12, while HNC/HCN 1-0 line ratio is 0.27 (Costagliola et al. 2011). Molecule lines of C₂H, CS, C¹⁸O, ¹³CO, CO at J = 1-0 transition and CN 1-0, as well as marginal detections of CH₃OH 5-4 and HC₃N 12-11 were reported in Costagliola et al. (2011) and Snell et al. (2011).

NGC 4258 (M106) is a Sab-type LINER/Seyfert galaxy at the distance of 6.8 Mpc (Tsai & Hwang 2015). Its anomalous spiral arms emerge from the galaxy nucleus and appear to intersect the regular spiral arms of galaxy (Ogle et al. 2014). Krause et al. (2007) reported that NGC4258 is a weak AGN and a pair of radio jets may be influencing the molecular emission. HCO⁺ 1-0, H41 α and ¹³CO 1-0 lines were reported in Snell et al. (2011), while Jiang et al. (2011) reported the detections of HCO, HCN, C₂H, HCO⁺ 1-0 and tentatively detected H¹³CO⁺ 1-0 at < 2 σ level. They both showed a very large HCO⁺/HCN ratio in NGC 4258.

NGC 6240 is a local ULIRG with extreme starburst activity and prominent AGN (Komossa et al. 2003) at the distance of 98 Mpc (Zhang et al. 2012), as merger of two AGN host galaxies. Observations showed that molecular emissions are concentrated in a small region between the two Seyfert nuclei (Wilson et al. 2008; Iono et al. 2007). Dense gas tracers including lines of HCN, HCO⁺, HNC and other molecular lines of CO, C₂H, HNCO, C¹⁸O and CN 1-0 had been detected, as well as tentatively detection of H¹³CN, SiO, H¹³CN and CH₃OH lines and HC₃N 10-9 and 12-11 were reported in Greve et al. (2009). Krips et al. (2008) and Costagliola et al. (2011) showed that the ratio of HCO⁺/HCN 1-0 was about 1.6 and suggested that HCO⁺/HCN is not a reliable tracer of XDRs.

VII Zw 31 is a gas-rich ULIRG (Fairclough 1986) at the distance of 240 Mpc (Leroy et al. 2011). It is a possible protogalactic disk at a low redshift and a merger-induced starburst (Djorgovski et al. 1990). This source had one of the

highest known CO luminosities and its molecule gas may be a large part of the dynamical mass (Sage & Solomon 1987; Radford et al. 1991). Detections of dense gas tracers of HCN 1-0 (Gao & Solomon 2004) and CS 5-4 (Wang et al. 2011) were also reported in literature. Downes & Solomon (1998) presented detections of CO 1-0 and 2-1 and tentatively detections of CN 1-0.

3 OBSERVATIONS AND DATA REDUCTION

Our observations toward four local galaxies were made with the IRAM 30 meter millimeter telescope at Pico Veleta, Spain¹, in December 2012. The setup of the observations were shown in Table 2. The Eight Mixer Receiver (EMIR) with dual-polarization and the Fourier Transform Spectrometers (FTS) backend with 8 GHz frequency coverage and 195 kHz frequency spacing were used. Standard wobbler switching mode with a $\pm 120''$ offset at 0.5 Hz beam throwing was used for the observations. Pointing was checked about every 2 hours with nearby strong millimeter emitting quasi-stellar objects. The EMIR receiver can provide two bands simultaneously. During the observations for each source with different days, we used 3 mm band with similar frequency tuning to cover mega-masers or red-shifted O₂ emission, while different frequency tuning setups were used at 1mm band to cover lines we were interested. The observational parameters are summarized in Table 2, with typical system temperature of about 137 K at 3 mm band and 142 K at 1mm band, including about 40 K from the receiver. About 12 hours observing time (on + off) were spent for each source of NGC 4258 and NGC 3079. Since they are the extremely nearby objects, the beam ($\sim 29''$ at 3mm) of IRAM 30 meter only covered the central region of NGC 4258 and NGC 3079. On the other hand, the observing time (on+off) toward VII Zw 31 and NGC 6240 is about 11 hours for each source. Emissions of our observations are from the entire galaxy for both VII Zw 31 and NGC 6240, as they are distant enough to be smaller than the beam of IRAM 30 meter telescope.

All the data were reduced with the CLASS package of GILDAS². We checked the line profile visually, and qualified spectra by comparing the measured noise and the theoretical noise before and after a few times of boxcar smooth. About 5% of the spectra were discarded during the qualification. We averaged them with time weighting and subtracted linear baselines for all spectra. We converted the antenna temperature (T_A^*) to the main beam brightness temperature (T_{mb}), using $T_{mb} = T_A^* \cdot F_{eff} / B_{eff}$, where F_{eff} and B_{eff} from the IRAM 30m homepage³ is tabulated in Table 1.

4 RESULTS

4.1 Detected Lines

A total of 33 molecular transitions were detected in these four galaxies with this observation. Two isotopic lines,

¹ Based on observations carried out with the IRAM 30m Telescope. IRAM is supported by INSU/CNRS (France), MPG (Germany) and IGN (Spain).

² <http://www.iram.fr/IRAMFR/GILDAS>

³ <http://www.iram.es/IRAMES/mainWiki/Iram30mEfficiencies>

Table 1. Telescope parameters from the IRAM 30m homepage ³

Observed Frequency	F_{eff}	B_{eff}
85GHz	0.95	0.81
111GHz	0.94	0.78
220GHz	0.92	0.59
217GHz	0.94	0.63
229GHz	0.92	0.59
248GHz	0.92	0.59
255GHz	0.87	0.49

H^{13}CN 1-0 and H^{13}CO^+ 1-0, were detected for the first time in NGC 4258, while these two lines, as isotopic lines of dense gas tracers, were not detected in NGC 3079, which can only give the upper limits (see Table 5). HC_3N was firstly detected in NGC 6240 with $J=29-28$ transition, while HNCO was firstly detected in VII Zw 31 with 12-11 transition. The observational parameters of each line were summarized in Table 5, 6, 7, and 8, including central velocity, line widths, peak intensity, velocity integrated intensity and column density. Lines with velocity integrated flux above 3σ level are considered as detections. The line identification was made using the Lovas (Lovas 1992) catalogues, and the Splatalogue data base⁴, which is a compilation of line lists including the Jet Propulsion Laboratory (Pickett et al. 1998). Informations of each source were described below.

For NGC 3079, as a composite source with both AGN and starburst, there are plenty of molecular lines in this source (See Figure A1 and Table 5). Normal dense gas tracers (HCO^+ 1-0, HCN 1-0, HNC 1-0, C_2H 1-0, and two groups of CN 2-1) were detected, as well as HNCO 4-3, CH_3CN 12₀-11₀ as new detections. Except for CH_3CN and ^{18}CO , other all species present a double peck structure (See Figure A1), which are consistent with that in the literature (Pérez-Beaupuits et al. 2007).

$\text{c-C}_3\text{H}_2$ 2-1, as well as isotopic lines of dense gas tracers, i.e., H^{13}CN 1-0, H^{13}CO^+ 1-0 (See Figure A2 and Table 6) were new detections in NGC 4258. However, CN 2-1 and C^{18}O lines were not detected.

HC_3N (29-28), which is optically thin and requires a dense and warm cloud component to excite, was firstly detected in NGC 6240 and showed a narrow line width of about 48 km s^{-1} (See Figure 2). Both red-shifted and blue-shifted line wings of CO 1-0 were detected in NGC 6240, which indicate possible molecular outflow from AGN in this source, which was consistent with the results in literature (Feruglio et al. 2013). For VII Zw 31, HNCO 12_{1,11}-11_{0,10} (see Figure A4 and Table 8) and C_2H 3-2 (see Figure 6) were detected as new results. While other molecular lines had been reported in literature for these two sources (See Table 7,8).

We compared the intensity ratio of HCO^+/HCN with the previous observation in these four sources, which suggested that the ratio of HCO^+/HCN might not be an ideal tool to identify AGN or starburst in galaxies.

⁴ www.splatalogue.net

4.2 Column densities

Local thermodynamic equilibrium (LTE) and optically thin emission for all the detected transitions were assumed to calculate the molecular column densities (N_{mol}) using the Boltzmann diagrams method (Goldsmith & Langer 1999), which needs at least two transitions of a given molecule to calculate the rotational temperatures. However, only one transition of each molecule was detected in our data for the four sources. A fixed T_{ex} was used for each source: 30 K for NGC 3079, 50 K for NGC 4258, 49 K for NGC 6240 (Braine et al. 1997; Cox & Downes 1996; Iono et al. 2007), and 49 K for VII Zw 31, which was adopted the same excitation temperature of NGC 6240 and was higher than the brightness temperature of 13 K from observation of CO (Radford et al. 1991), were used to calculate the column densities. The data also were corrected by the beam dilution effect, as $T_B = [(\theta_s^2 + \theta_b^2) / \theta_s^2] \times T_{MB}$, where T_B is the source average brightness temperature, θ_s is the source size, θ_b is the beam size in arc seconds, and T_{MB} is the measured main beam temperature. Based on the four sources interferometric observations of CO (1-0) for NGC 3079 (Koda et al. 2002), CO (2-1) NGC 4258 (Sawada-Satoh et al. 2007), CO (1-0) for NGC 6240 (Feruglio et al. 2013), CO (1-0), CO (2-1) for VII Zw 31 (Downes & Solomon 1998), we roughly assumed the sizes of $11''$ and $8''$ for the nuclear regions of NGC 3079 and NGC 4258; $3''$ and $4''$ for NGC 6240 and VII Zw 31, respectively.

At LTE and optically thin conditions, we have

$$N_u = \frac{8\pi k \nu^2 W}{hc^3 A_{ul}} \quad (1)$$

where N_u is the upper state column density of the molecule, W is the integrated brightness temperature, k is the Boltzmann constant, ν is the frequency of the transition, h is the Planck constant and A_{ul} is the Einstein's transition probability coefficients. The spectroscopic parameters were obtained from the Cologne Database for Molecular Spectroscopy (CDMS; Müller et al. (2005)) and JPL catalogs (Pickett et al. 1998).

$$N_u = \frac{N}{Q(T_{ex})} g_u e^{-E_u/kT_{ex}} \quad (2)$$

where N is the total number density of molecules, $Q(T_{ex})$ is the partition function, g_u is the degeneracy of the upper state and E_u is the upper level energy. The partition function $Q(T_{ex})$ of each molecule is calculated by fitting the partition function at different temperature from CDMS.

The column densities for all molecules were showed in Tables 5, 6, 7, and 8. Note that although we assumed all lines are optically thin for calculation, some lines are certainly optical thick, such as HCN and HCO^+ in NGC 3079 and NGC 4258 (See Table 4), for which the column densities were underestimated. Ratios of column densities for the four sources were calculated and listed in Table 9.

5 DISCUSSIONS

5.1 NGC 3079 v.s. NGC 4258: AGN and starburst hybrid v.s. pure AGN

As mentioned in §3, the IRAM beams can not cover the entire galaxy for both NGC 3079 and NGC 4258, which cause

Table 2. Observational parameters

Source	RA (J2000)	DEC (J2000)	Band range (GHz)	Tsys (K)	Time (min)	RMS (mK)	δ_v (km s ⁻¹)
NGC3079	10:01:57.80	55:40:47.0	85-92	114	115	4	0.7
			220-227	260	131	13	0.3
NGC4258	12:18:57.50	47:18:14.0	85-92	101	650	2	0.7
			219-227	210	102	8	0.3
			229-236	151	122	10	0.3
NGC6240	16:52:58.90	02:24:03.0	111-120	167	175	6	0.2
			260-268	232	100	15	0.5
VIIIZW31	05:16:45.10	79:40:13.0	112-117	117	89	5	0.5
			228-236	292	145	13	0.3
			260-268	198	110	11	0.2

Notes. The broad-band observations include 1 mm and 3 mm band. δ_v is the velocity resolution of the molecular lines relative to 195 kHz frequency resolution, while the 'RMS' in each line was obtained with 'base' at this velocity resolution.

Table 3. Line ratios

Sources	$\frac{I_{1-0}^{HCO^+}}{I_{1-0}^{HCN}}$	$\frac{I_{1-0}^{HCO^+}}{I_{1-0}^{HCN}}$	$\frac{I_{1-0}^{HNC}}{I_{1-0}^{HCN}}$	$\frac{I_{3-2}^{HCO^+}}{I_{3-2}^{HCN}}$	$\frac{I_{29-28}^{HC_3N}}{I_{3-2}^{HCN}}$	$\frac{I_{10-9}^{HC_3N}}{I_{1-0}^{HCN}}$
NGC 3079	3.17 ± 0.51	0.96 ± 0.11	0.30 ± 0.04	< 0.03
NGC 4258	6.88 ± 0.69	1.99 ± 0.06	0.29 ± 0.03	0.11 ± 0.03
NGC 6240	1.48 ± 0.08	0.03 ± 0.01	...
VII Zw 31	0.78 ± 0.15	< 0.2	...

Literature Data						
Sources	$\frac{I_{3-2}^{HCO^+}}{I_{3-2}^{HCN}}$	$\frac{I_{1-0}^{HCO^+}}{I_{1-0}^{HCN}}$	$\frac{I_{1-0}^{HNC}}{I_{1-0}^{HCN}}$	$\frac{I_{10-9}^{HC_3N}}{I_{1-0}^{HCN}}$	Type	Reference
NGC 1068	0.38 ± 0.07	0.60 ± 0.01	AGN	1
NGC 4388	...	1.38 ± 0.4	0.62 ± 0.24	< 0.35	AGN	2
NGC 5194	< 0.7	0.72 ± 0.06	AGN	1
NGC 7469	...	1.12 ± 0.11	0.55 ± 0.08	< 0.07	AGN	2
NGC 2273	...	1.05 ± 0.37	1.09 ± 0.38	< 0.89	AGN	2
NGC 4826	< 0.7	0.59 ± 0.04	AGN+SB	1
NGC 3627	< 0.7	1.0 ± 0.1	AGN+SB	1
NGC 4569	< 0.9	0.85 ± 0.07	AGN+SB	1
NGC 6951	< 0.8	0.7 ± 0.05	AGN+SB	1
NGC 6946	0.94 ± 0.08	0.86 ± 0.07	SB	1
NGC 2146	1.2 ± 0.2	1.3 ± 0.08	SB	1
M 82(center)	0.7 ± 0.2	1.5 ± 0.04	SB	1
NGC 1614	...	1.83 ± 0.37	0.33 ± 0.15	< 0.35	SB	2
NGC 4194	...	1.32 ± 0.32	0.53 ± 0.23	< 0.20	SB	2
NGC 660	...	1.04 ± 0.09	0.52 ± 0.06	< 0.07	SB	2
NGC 3556	...	1.57 ± 0.37	0.37 ± 0.24	< 0.27	SB	2
NGC 6240	0.7 ± 0.2	1.6 ± 0.2	ULIRG(AGN+SB)	1
Mrk 231	0.4 ± 0.1	0.87 ± 0.09	ULIRG(AGN+SB)	1
Arp 220	0.2 ± 0.05	0.48 ± 0.05	ULIRG(AGN+SB)	1
NGC 4418	...	0.59 ± 0.1	0.47 ± 0.09	< 0.18	LIRG(AGN)	2

1 Data taken from [Krips et al. \(2008\)](#).

2 Data taken from [Costagliola et al. \(2011\)](#).

Our result shown that the ratio of HCO⁺/HCN (J = 3-2) in NGC 6240 is different from [Krips et al. \(2008\)](#) reported.

that the detected emissions are mainly from the nuclear region.

5.1.1 Molecules

The comparison of molecular abundances among these two galaxies was shown in Figure 3. HNCO $4_{0,4} - 3_{0,3}$ at 87.925 GHz, CH₃CN $12_0 - 11_0$ at 220.747 GHz, H₂CO $3_{1,2} - 2_{1,1}$ at

225.698 GHz, and the two CN 2-1 lines at 226.66 GHz and 226.875 GHz, were detected only in NGC 3079. Starburst active in NGC 3079 may enhanced the abundances of these species. Since NGC 3079 is more distant than NGC 4258, the intrinsic luminosities of these line emissions are significantly higher than the upper limits in NGC 4258. Shock gas tracer and dense gas tracer are detected in NGC 3079, such as HNCO and CH₃CN, as well as PDR tracer H₂CO. The

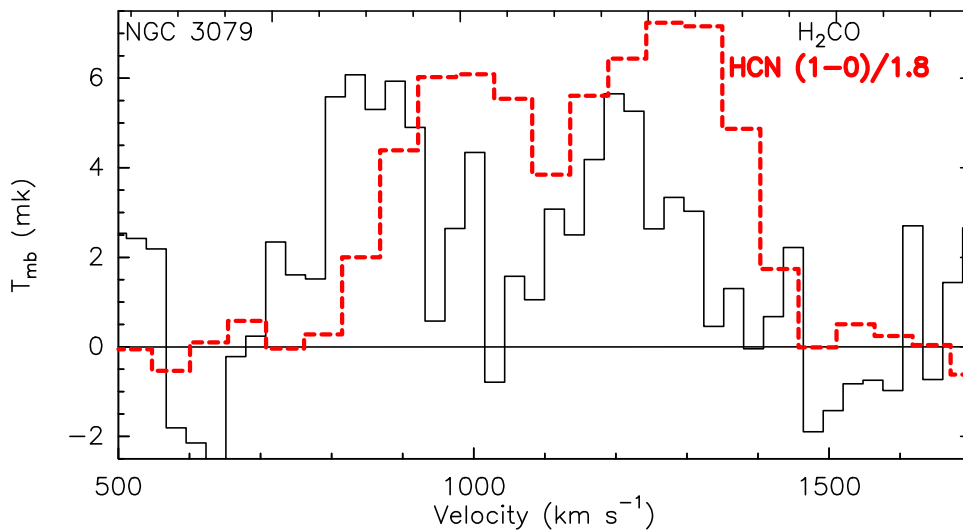


Figure 1. Two emission features near 225.7 GHz with identification as H_2CO ($3_{1,2} - 2_{1,1}$) (black line), overlaid with HCN (1-0) divided by 1.8 (red line).

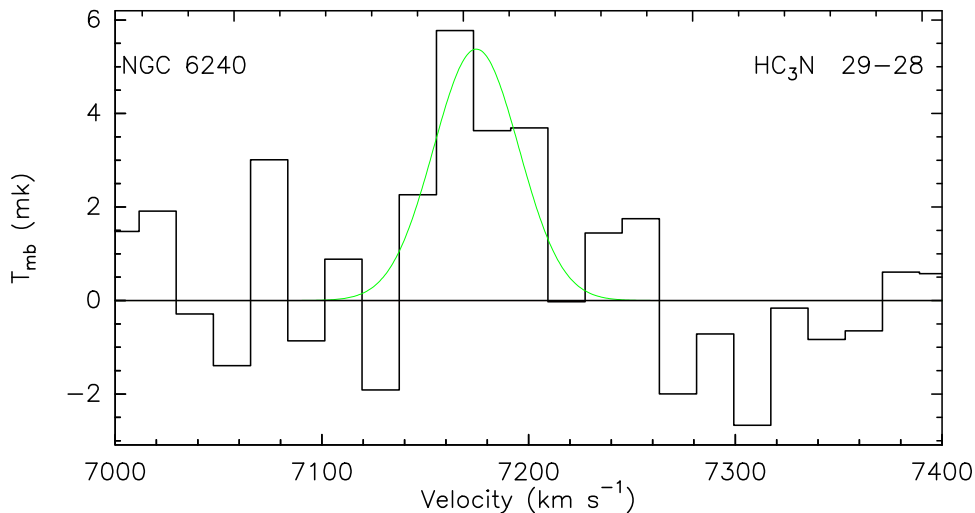


Figure 2. HC_3N 29-28 line detected in NGC 6240, with rms of 1.07 mK at the velocity resolution of 23.97 km s^{-1} , overlaid with Gaussian fitting (green line).

relative abundances of C_2H , HNCO , HCN , HCO^+ and HNC to CN are similar to that in NGC 253 (Aladro et al. 2015), which implies that the environment of starburst in NGC 3079 might be similar to that in NGC 253. NGC 3079 may be in an intermediate starburst stage, with an active starburst. Shock gas tracer HNCO had higher abundances than PDR tracers $c\text{-C}_3\text{H}_2$ in NGC 3079. All above species had also been detected toward nearby starburst galaxy M82 (Aladro et al. 2011) and the nearest ULIRGs Arp 220 (Martín et al. 2011).

On the other hand, the faint lines of H^{13}CN 1-0, H^{13}CO^+ 1-0, and SiO 2-1, were only detected in NGC 4258. The velocity integrated intensity and line center of SiO 2-1 of NGC 4258 is similar to that of Wang et al. (2013), but with broader line width. SiO usually trace shocks in extragalactic sources (García-Burillo et al. 2000, 2001) and its abundance may be enhanced by X-ray chemistry in AGNs (Aladro et al. 2013). That is, SiO is somehow expected to be detected in NGC 3079, which have strong active AGN and shock gas. However, it was not detected at similar noise level of NGC 4258. All of the lines detected in NGC 3079 and NGC 4258 had been detected as strong emission lines in Orion A with

line survey (Sutton et al. 1985). It is interesting that CN 2-1 in NGC 4258 as a pure AGN was not detected, which was contrary to models showed by Meijerink et al. (2007). While the strong emission of CN 2-1 was detected in NGC 3079 (SB+AGN), in which CN might be enhanced not only in XDRs, but also PDRs near massive young stars (Aalto et al. 2002). C_2H 1-0 emissions were also detected in NGC 4258 and NGC 3079. However, the 6 hyperfine structures can not be separated due to the line broadening (See Figure 5).

5.1.2 The line profiles

The line parameters for NGC 3079 and NGC 4258, including velocity-integrated flux, line velocity and line width, are summarized in Table 5, 6. For NGC 3079, except for CH_3CN and ^{18}CO , other all species have showed obviously two separated velocity components, which is consistent with the results in literature (Pérez-Beaupuits et al. 2007) (See Figure 7). It indicates that two components with different velocities exist in this source. ^{18}CO 2-1 may be a double peak structure. However, it is at the edge of the band, which causes

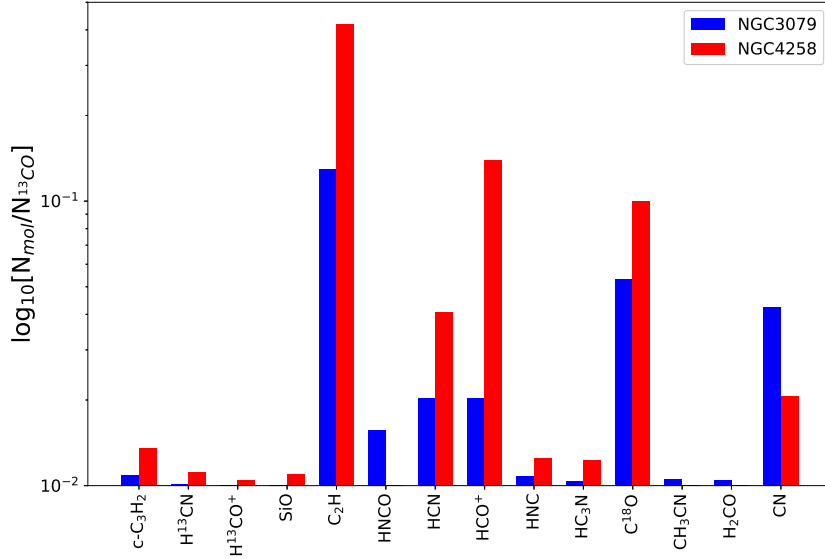


Figure 3. Comparison between NGC 3079 and NGC 4258 fractional abundances of different molecules with respect to the ^{13}CO abundances. For ^{18}CO , the lower limit just be shown in NGC 4258, while CO is not shown here because it is off the chart.

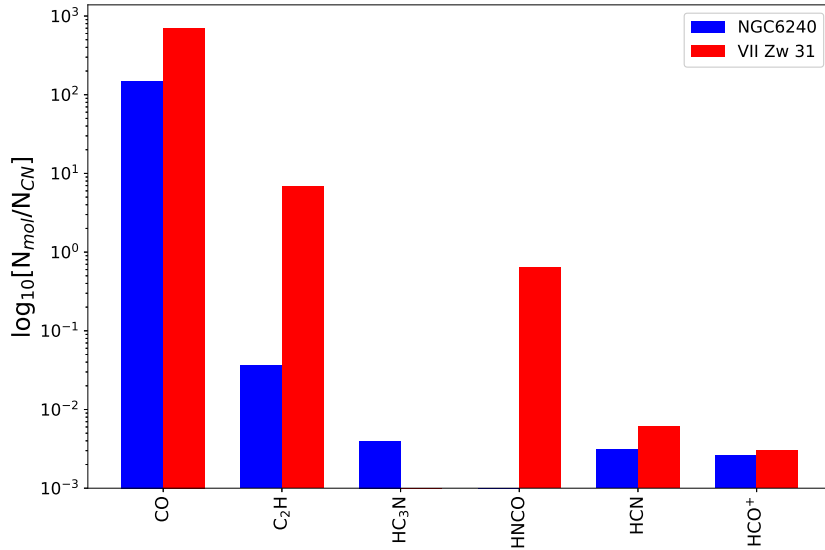


Figure 4. Comparison between NGC 6240 and VII Zw 31 fractional abundances of different molecules with respect to the CN abundances.

only the blue-shifted component was detected, while the red-shifted component was out of the frequency coverage. Based on profiles of other lines, such as HCN 1-0 and HCO⁺ 1-0, ^{13}CO 2-1 should have two components velocity. However, it is hard to distinguish the double peak structure, due to the high opacity. CH₃CN could have two velocity components. However, we can not distinguish CH₃CN emission profile due to the red-shifted component of CH₃CN is blended by ^{13}CO 2-1. On account of most of red-shift component of molecular lines were detected in NGC 3079, we used line widths of red-component of HCN 1-0 to estimate upper limit of integrated

intensities for HC₃N 10-9 and H¹³CN 1-0, while use that of HCO⁺ 1-0 for H¹³CO⁺ 1-0.

For NGC 4258, we find that except for H¹³CN, H¹³CO⁺, H₃CN and SiO, the central velocity of other species is about 450 km/s and the line width is about 250 km/s. H¹³CO⁺ and H¹³CN are just detected around 3σ level, which may cause the uncertainty of estimating velocity.

5.1.3 Line ratios

The ratios of HCO⁺/HCN, HCO⁺/HNC, and HCN/HNC were listed in Table 3. HCO⁺/HCN line ratio had been

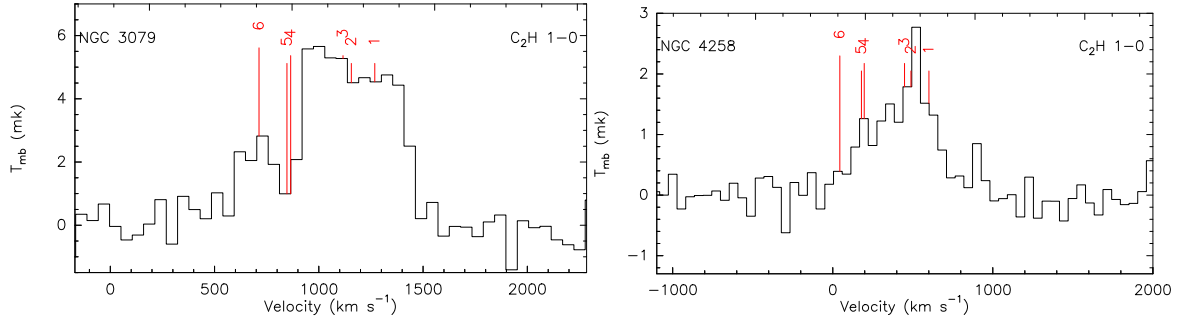


Figure 5. C_2H (1-0) detected in NGC 3079 and NGC 4258. The rms is 0.55 mK at the velocity resolution of 54.31 km s^{-1} in NGC 3079 and 0.25 mK at the velocity resolution of 54.31 km s^{-1} in NGC 4258. The same six hyperfine lines are marked from 1-6 in these two sources: 1, C_2H 1-0 $3/2-1/2$ $F=1-1$ at 87284.15GHz; 2, C_2H 1-0 $3/2-1/2$ $F=2-1$ at 87316.92GHz; 3, C_2H 1-0 $3/2-1/2$ $F=1-0$ at 87328.62GHz; 4, C_2H 1-0 $1/2-1/2$ $F=1-1$ at 87402.00GHz; 5, C_2H 1-0 $1/2-1/2$ $F=0-1$ at 87407.16GHz; 6, C_2H 1-0 $1/2-1/2$ $F=1-0$ at 87444.47GHz. The transition of $J=1-0$ $3/2-1/2$ $F=1-0$ is used as reference for the velocities in these two galaxies.

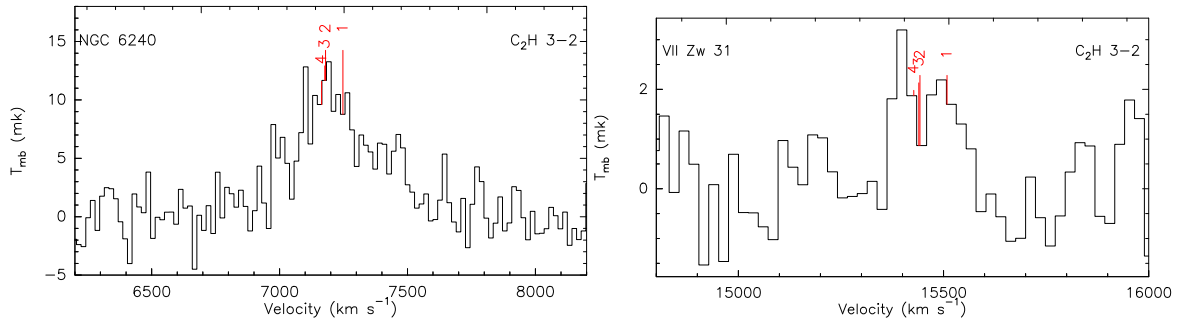


Figure 6. C_2H (3-2) detected in NGC 6240 and VII ZW 31. The rms is 1.89m K at the velocity resolution of 18.1 km s^{-1} in NGC 6240 and 1.18 mK at the velocity resolution of 18.10 km s^{-1} . The same four hyperfine lines are marked from 1-4 in these two sources: 1, C_2H 3-2 $J=7/2-5/2$ $F=4-3$ at 262.004 GHz; 2, C_2H 3-2 $J=5/2-3/2$ $F=3-2$ at 262.065 GHz; 3, C_2H 3-2 $J=5/2-3/2$ $F=2-1$ at 262.067 GHz, 4, C_2H 3-2 $J=5/2-3/2$ $F=2-2$ at 262.079 GHz. The transition of $J=5/2-3/2$ $F=2-1$ is used as reference for the velocities in these two galaxies.

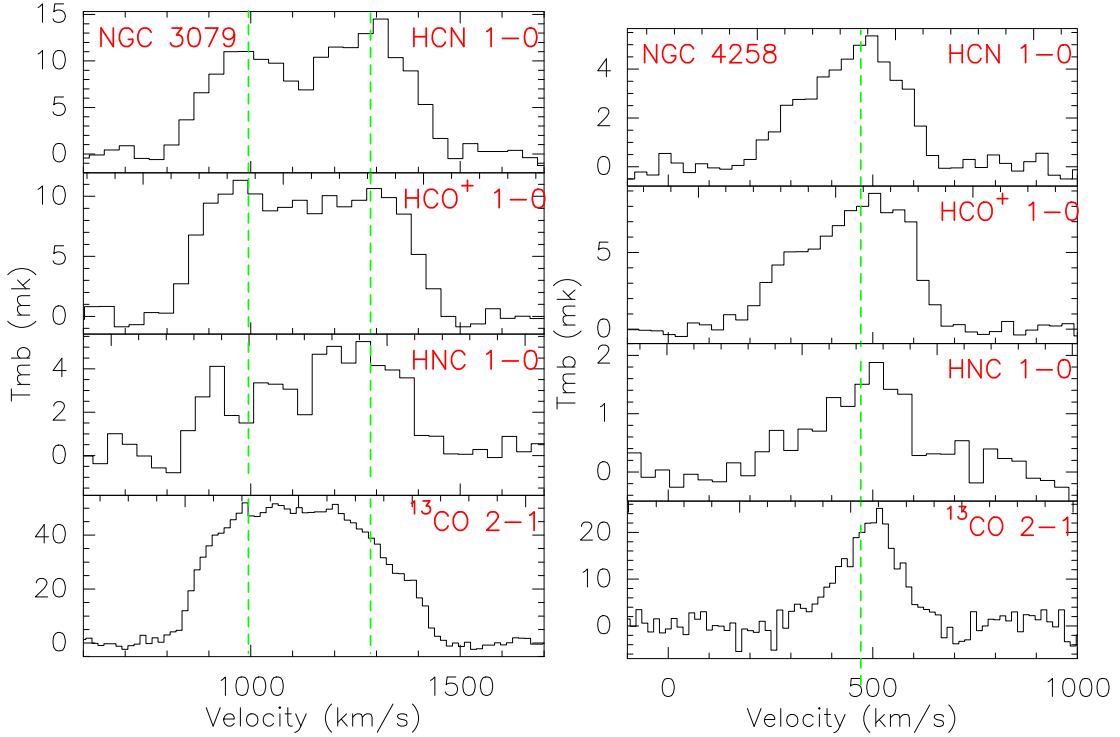


Figure 7. Spectra lines in NGC 3079 and NGC 4258.

used to distinguish between AGNs and starburst signatures in galactic centers (Kohno et al. 2001; Imanishi et al. 2007; Krips et al. 2008). As a result in literature, HCO⁺/HCN in starburst and LIRGs was higher than that in AGN, explained by the enhancement of HCN abundance in XDR surrounding an AGN (Costagliola et al. 2011; Privon et al. 2017). Furthermore, an enhanced intensity of HCN (1-0), with respect to HCO⁺ (1-0) in the studies of AGN dominated galaxies, was interpreted as evidence for the influence of X-ray dominated regions (XDRs) or mechanical heating (Izumi et al. 2016). But there are some counterarguments to this statement that lower line ratio of HCO⁺/HCN, which were reported in pure starburst and composite galaxies (Costagliola et al. 2011; Privon et al. 2015). Mills et al. (2013) presented that low HCO⁺/HCN ratio was also found in individual galactic star-forming regions. Although many different effects can contribute to an HCN enhancement in active environments, the actual cause is not clear.

Izumi et al. (2013, 2016) concluded that the high abundances and mechanical heating from a jet or shock could drive the HCN enhancement relative to HCO⁺ in AGN galaxies. While, in our observations, the high line ratio of HCO⁺/HCN 1-0 (~ 2) in NGC 4258, which is consistent with that in Jiang et al. (2011), is different to the typical value of pure AGNs (Krips et al. 2008). Different optical depth of these two molecules might play a key role in this ratio. The opacity of HCN was almost twice of HCO⁺ (see Table 4). On the other hand, the lower critical densities of HCO⁺ than that of HCN, may cause that HCO⁺ region from the relative low density gas. This scenario is equivalent to that discussed toward local starbursts galaxies for the high HCO⁺/HCN ratio (Meier & Turner 2012). The ratio of HCO⁺/HCN in NGC 3079 was consistent with that in Costagliola et al. (2011), similar to that in other AGN/starburst composite sources in literature (Krips et al. 2008).

Since the red-shifted component of C¹⁸O 2-1 was out of frequency coverage, we just use peak temperature to estimate the ratio of ¹³CO/ C¹⁸O as 3.5. On the other hand, based on the non-detection of C¹⁸O 2-1, the lower limit of this ratio in NGC 4258 is about 11. The different line ratios of ¹³CO/C¹⁸O in these two galaxies might due to different isotopic ratios of ¹³C/¹²C and ¹⁶O/¹⁸O, or self-absorption of ¹³CO 2-1 in NGC 3079.

With better sensitivity than that of Jiang et al. (2011), we marginally detected H¹³CO⁺ and H¹³CN for the first time above 3 σ level in NGC 4258. HCN 1-0 and HCO⁺ 1-0 overlaid on their isotopic lines are presented in Figure 8. With assumption that the isotopic ratios of molecules are the same as the isotopic abundance of ¹²C/¹³C and this ratio is 40, which was suggested for nearby galaxies (Henkel et al. 1993, 2014; Aladro et al. 2013), we can calculate the optical depths of HCO⁺ 1-0 and HCN 1-0, with $R = \frac{1 - e^{-\tau_{12}}}{1 - e^{-\tau_{13}}}$, where R is the detected line intensity ratio and τ is the optical depth. We obtained the optical depths for NGC 4258, and the upper limits for NGC 3079, respectively. The values of two sources has been showed in Table 4. The optical depths are similar to that in nuclear region of nearby type II Seyfert galaxy NGC 1068, with the optical depths of HCN 1-0 and HCO⁺ 1-0 as 4.6 and 3.0, respectively (Wang et al. 2014). The optically thick lines of HCN and HCO⁺ can not well distinguish the abundance ratio of HCO⁺/HCN due to

self absorption. Isotopic lines of dense gas tracers in galaxies can help us to derive the optical depths of dense gas tracers, which is important to accurate the relationship between the dense gas and the star formation (Gao & Solomon 2004), especially for individual galaxies. Krips et al. (2008) showed that IR pumping is not significantly to effect the HCO⁺-to-HCN intensity ratios. Line ratio of optically thin isotopologues (H¹³CO⁺/H¹³CN), which is more related to the relative abundances than that of HCO⁺/HCN with assumption of similar excitation temperatures, is larger than unity in NGC 4258.

5.2 NGC 6240 v.s. VII Zw 31: AGN and extreme starburst hybrid v.s. extreme starburst

NGC 6240 and VII Zw 31 are about ten times more distant than NGC 3079 and NGC 4258. The IRAM beams covered the entire galaxy for both NGC 6240 and VII Zw 31.

5.2.1 Molecules

The detected lines in these two sources are similar, including CN 1-0, CO 1-0, C₂H 1-0, HCN 3-2, and HCO⁺ 3-2, except that HC₃N 29-28 line was only detected in NGC 6240 and HNCO 12-11 was only detected in VII Zw 31. Although we did not detect new extragalactic molecules in these two sources, HNCO and HC₃N 29-28 was detected for the first time in VII Zw 31 and NGC 6240, respectively. The detected species are listed in Tables 7 and 8. Figure 4 show the comparison of molecular abundances among these two galaxies. Two groups of CN 1-0 lines, which include nine hyperfine transitions, were detected both in NGC 6240 and VII Zw 31. Due to the line broadening of galaxies, the nine CN 1-0 lines were in two groups, five of which were around 113.491 GHz while four of which were around 113.191 GHz. The detected CN_{113.491GHz} / CN_{113.191GHz} ratios in NGC 6240 and VII Zw 31 were about 2, which were similar to the optical depth ratio of the two groups and indicated that the lines were optically thin. C₂H 3-2 was detected in these two sources. However, due to the line broadening, the 4 hyperfines can not be resolved (See Figure 6).

Some transitions of HC₃N in galaxies had been detected (Aladro et al. 2011; Costagliola et al. 2011; Lindberg et al. 2011; Jiang et al. 2017), with low detection rate. So far, HC₃N 32-31 in NGC 4418 was the highest transition detected in external galaxies (Costagliola et al. 2015). With the detection of HC₃N 29-28, which requires the excitation conditions with high density (around 10⁶ cm⁻³) and high temperature ($E_u \sim 190$ K) (Aladro et al. 2015), at least part of molecular gas in NGC 6240 should have similar physical properties to that in NGC 4418. HNCO, as a good tracer of the evolution of nuclear SB in galaxies and a shock tracer (Aladro et al. 2015; Martín et al. 2008), was detected in VII Zw 31, which implied that the ISM of VII Zw 31 might be dominated by shocks affecting the molecular clouds fueling the SB.

5.2.2 Line ratios

The line ratio of HCO⁺/HCN 3-2 was 1.5 in NGC 6240, which was about twice of the value in Krips et al. (2008).

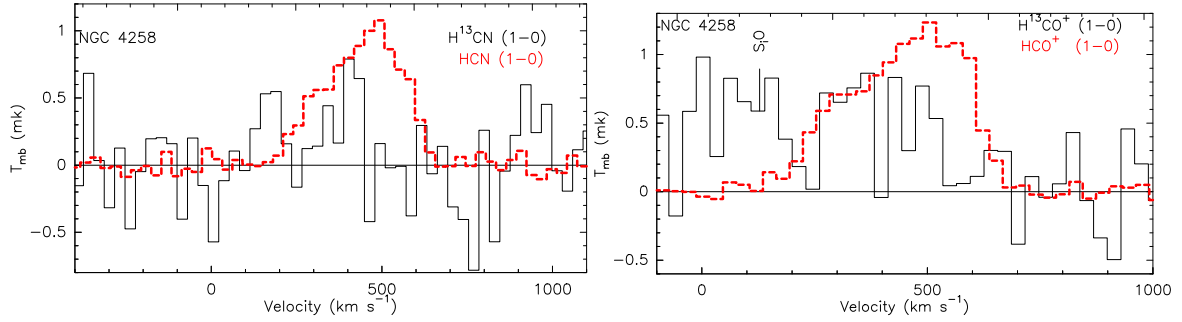


Figure 8. Isotopologue lines of dense-gas tracers detected in NGC 4258. Left: H^{13}CN (1-0) (black line) overlaid with HCN (1-0) multiplied by 5 (red line). Right: H^{13}CO^+ (1-0) (black line) overlaid with HCO^+ (1-0) multiplied by 7.2 (red line). The SiO 2-1 line is also detected, which is at left of H^{13}CO^+ (1-0).

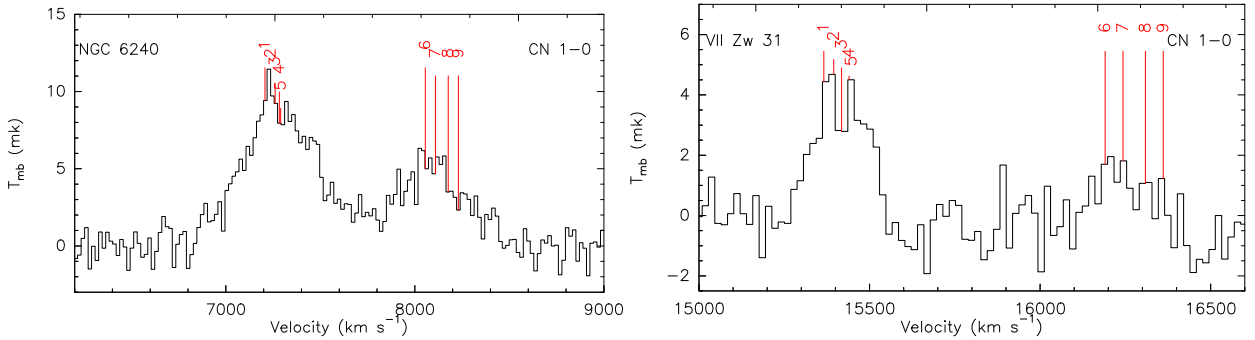


Figure 9. CN (1-0) in NGC 6240 and VII ZW 31. The rms is 0.88 mK at the velocity resolution of 18.57 km s^{-1} in NGC 6240 and 0.99 mK at the velocity resolution of 18.57 km s^{-1} . The same nine hyperfine lines are marked from 1-9 in these two sources: 1, CN 1-0 $J=3/2-1/2$ $F=1/2-3/2$ at 113.520 GHz; 2, CN 1-0 $J=3/2-1/2$ $F=3/2-3/2$ at 113.509 GHz; 3, CN 1-0 $J=3/2-1/2$ $F=1/2-1/2$ at 113.4996 GHz; 4, CN 1-0 $J=3/2-1/2$ $F=5/2-3/2$ at 113.491 GHz; 5, CN 1-0 $J=3/2-1/2$ $F=3/2-1/2$ at 113.488 GHz; 6, CN 1-0 $J=1/2-1/2$ $F=3/2-3/2$ at 113.191 GHz; 7, CN 1-0 $J=1/2-1/2$ $F=3/2-1/2$ at 113.171 GHz; 8, CN 1-0 $J=1/2-1/2$ $F=1/2-3/2$ at 113.144 GHz; 9, CN 1-0 $J=1/2-1/2$ $F=1/2-1/2$ at 113.123 GHz. The transition of $J=3/2-1/2$ $F=1/2-3/2$ in NGC 6240 and $J=3/2-1/2$ $F=5/2-3/2$ in VII Zw 31 is used as reference for the velocities, respectively.

Table 4. Derived optical depths for NGC 4258 and the upper limits for NGC 3079

Source	$\tau(\text{HCN}1-0)$	$\tau(\text{H}^{13}\text{CN}1-0)$	$\tau(\text{HCO}^+1-0)$	$\tau(\text{H}^{13}\text{CO}^+1-0)$
NGC 3079	< 1.2	< 0.07	< 1.0	< 0.07
NGC 4258	4.6 ± 1.2	0.12 ± 0.03	3.0 ± 0.6	0.08 ± 0.02

HCO^+ and HCN data from the observation at different time in Krips et al. (2008), with HCO^+ data from Graciá-Carpio et al. (2006). The velocity integrated intensity of HCN 3-2 in our results was almost the same as that in Krips et al. (2008), while it was more than twice flux in our results than that of Krips et al. (2008) for HCO^+ . The pointing error can underestimate flux of HCO^+ , resulting in underestimating line ratio of HCO^+/HCN . The ratio was 0.78 for VII Zw 31, as a typical value for ULIRGs (Costagliola et al. 2011). While the higher HCO^+/HCN 3-2 ratio in NGC 6240 is close to SB-dominated source, as seen in starburst-dominant galaxy nuclei. With two prominent AGN in NGC 6240, we suggest that an enhanced HCN abundance in an AGN could be the reason for the higher HCN flux, resulting in higher HCO^+/HCN 3-2 in NGC 6240 than VII Zw 31, in which no obvious AGN signature exists.

5.3 Comparison with observations in literature

The derived ratios of HCO^+/HCN agree well with previous studies for NGC4258 (Jiang et al. 2011) and NGC

3079 (Krips et al. 2008; Costagliola et al. 2011), while it is about twice for NGC 6240 than that in Krips et al. (2008). HCO^+/HCN 3-2 ratio is a new measurement for VII Zw 31. More HCO^+/HCN ratios for other sources from the literature are listed in Table 3, which show that starbursts have, on average, higher HCO^+/HCN ratios than AGN. The HCO^+/HCN ratio can be used to observationally distinguish AGN-important and starburst-dominant galaxy nuclei. For the composite sources (NGC 6240 and NGC 3079), we found that this ratio is moderately low comparing to starburst galaxies. We suggest that the line intensity may be contaminated from coexisting AGN region have a lower HCO^+/HCN ratio. This indicates that the HCO^+/HCN may not be a perfect diagnostic tool between AGN and SB environments, due to combination of both processes.

5.4 $\text{HC}_3\text{N}/\text{HCN}$

Table 3 show upper limit of $\text{HC}_3\text{N}/\text{HCN}$ ratio from literature. The starburst galaxies are, on average, lower $\text{HC}_3\text{N}/\text{HCN}$ ratios comparing with AGNs. It is consistent

Table 5. Detected lines in NGC 3079

Molecule	Frequency GHz	$\int T_{mb} dv$ (K km s ⁻¹)	v_{LSR} (km s ⁻¹)	FWHM (km s ⁻¹)	Column densities ($\times 10^{13}$ cm ⁻²)
c-C ₃ H ₂ (2 _{1,2} - 1 _{0,1})	85.339	< 0.11(3 σ) ^a	...	113.3	< 2.7
		0.31 \pm 0.05 ^b	1276.8 \pm 10.3	113.3 \pm 20.3	...
H ¹³ CN (1-0)	86.342	< 0.25(3 σ)	...	231.8	< 0.52
H ¹³ CO ⁺ (1-0)	86.754	< 0.22(3 σ)	...	254.0	< 0.15
C ₂ H (1-0)	87.329	3.54 \pm 0.17	1117	554.7	380 \pm 18
HNCO (4 _{0,4} - 3 _{0,3})	87.925	0.22 \pm 0.06 ^a	876.3 \pm 13.7	103.9 \pm 37.3	18 \pm 4.9
		0.21 \pm 0.08 ^b	1223.8 \pm 48.7	242.7 \pm 81.4	...
HCN (1-0)	88.631	2.45 \pm 0.15 ^a	987.2 \pm 6.7	205.7 \pm 13.0	33 \pm 0.84
		3.40 \pm 0.15 ^b	1277.3 \pm 5.7	231.8 \pm 11.5	...
HCO ⁺ (1-0)	89.189	2.64 \pm 0.41 ^a	989.1 \pm 16.9	223.7 \pm 30.2	33 \pm 2.4
		2.97 \pm 0.41 ^b	1265.1 \pm 20.7	254.0 \pm 32.8	...
HNC (1-0)	90.663	0.52 \pm 0.28 ^a	973.2 \pm 36.7	187.0 \pm 97.3	2.5 \pm 0.42
		1.25 \pm 0.31 ^b	1257.1 \pm 20.2	243.8 \pm 68.9	...
HC ₃ N (10-9)	90.979	< 0.20(3 σ)	...	231.8	< 1.3
C ¹⁸ O (2-1)	219.560	> 1.32 \pm 0.21	968.9 \pm 12.1	139.6 \pm 21.8	> 138 \pm 22
¹³ CO (2-1)	220.399	31.86 \pm 0.26	1112.1 \pm 1.7	408.5 \pm 3.4	3191 \pm 26
CH ₃ CN (12 ₀ - 11 ₀)	220.747	0.95 \pm 0.17	935.4 \pm 13.9	145.2 \pm 28.2	1.6 \pm 0.29
H ₂ CO (3 _{1,2} - 2 _{1,1})	225.698	1.09 \pm 0.19	860.9 \pm 14.7	172.7 \pm 35.3	1.5 \pm 0.14
		0.98 \pm 0.20	1208.0 \pm 18.3	193.3 \pm 51.2	...
CN (2-1)	226.660	2.06 \pm 0.16 ^a	973.9 \pm 5.8	144.1 \pm 11.7	103 \pm 2
		0.66 \pm 0.14 ^b	1299.3 \pm 12.5	113.8 \pm 23.3	...
CN (2-1)	226.875	2.62 \pm 0.20 ^a	983.3 \pm 2.1	193.2 \pm 17.2	...
		3.47 \pm 0.20 ^b	1250.4 \pm 1.4	180.2 \pm 11.5	...

Notes. The fluxes are in T_{mb} instead of T_A . For C₂H, the hyperfine transition, the flux integrated from 514 km s⁻¹ to 1596 km s⁻¹. c-C₃H₂, HNCO, HCN, HCO⁺, HNC and CN show a double peaked structure. a and b is the two Gaussian components. We use the red-shift component line width to estimate upper integrated intensity limit the blue-shift component of c-C₃H₂. We estimate upper integrated intensity limit of HC₃N, H¹³CN with the red-shift component line width of HCN and H¹³CO⁺ with the red-shift component line width of HCO⁺, respectively. The column densities were calculated with the correction of an estimated source size.

Table 6. Detected lines in NGC 4258

Molecule	Frequency GHz	$\int T_{mb} dv$ (K km s ⁻¹)	v_{LSR} (km s ⁻¹)	FWHM (km s ⁻¹)	Column densities ($\times 10^{13}$ cm ⁻²)
c-C ₃ H ₂ (2 _{1,2} - 1 _{0,1})	85.339	0.11 \pm 0.03	459.1 \pm 15.9	126.6 \pm 33.6	2.4 \pm 0.65
H ¹³ CN (1-0)	86.342	0.14 \pm 0.04	391.4 \pm 17.5	327.6 \pm 93.2	0.79 \pm 0.23
H ¹³ CO ⁺ (1-0)	86.754	0.17 \pm 0.05	388.5 \pm 40.2	277.1 \pm 99.3	0.32 \pm 0.09
SiO (2-1)	86.847	0.12 \pm 0.04	389.5 \pm 29.5	177.8 \pm 50.0	0.65 \pm 0.22
C ₂ H (1-0)	87.329	0.96 \pm 0.07	459.9 \pm 16.6	494.2 \pm 40.2	280 \pm 20
*HCN (1-0)	88.631	1.38 \pm 0.04	451.0 \pm 3.3	266.6 \pm 7.3	21 \pm 0.61
*HCO ⁺ (1-0)	89.189	2.75 \pm 0.04	459.1 \pm 2.4	308.9 \pm 5.3	89 \pm 1.3
*HNC (1-0)	90.663	0.40 \pm 0.04	482.9 \pm 10.4	247.7 \pm 35.0	1.7 \pm 0.17
HC ₃ N (10-9)	90.979	0.11 \pm 0.03	561.9 \pm 23.6	232.1 \pm 94.8	1.6 \pm 0.44
C ¹⁸ O (2-1)	219.560	< 0.33(3 σ)	...	162.5	< 62
¹³ CO (2-1)	220.399	3.79 \pm 0.18	495.0 \pm 3.7	162.5 \pm 9.2	687 \pm 33
CN (2-1)	226.660	< 0.17(3 σ)	...	264.4	< 7.3
CN (2-1)	226.875	< 0.18(3 σ)	...	264.4	...
*CO (2-1)	230.538	80.90 \pm 0.15	485.6 \pm 0.2	209.3 \pm 0.5	14272 \pm 26

The fluxes are in T_{mb} instead of T_A . For C₂H, the hyperfine transition, the flux integrated from -69 km s⁻¹ 1166 km s⁻¹. We use line width of HCN to estimate upper integrated intensity limit of CN. The asterisk * shows lines are optically thick and their column density would be underestimated. The column densities were calculated with the correction of an estimated source size. We estimate upper limits of CN 2-1 and C¹⁸O 2-1 integrated intensities with line width of HCN and ¹³CO, respectively.

with Lindberg et al. (2011), which concluded that starburst galaxies seem to be poor in HC₃N, because HC₃N is easily dissociated by UV radiation. As mentioned in Sec. 5.2.1, HC₃N 29-28 was detected in NGC 6240 with the ratio of HC₃N 29-28/HCN 3-2 of 0.03, which gave that HC₃N

abundance of NGC 6240 was lower than that of other two ULIRGs: Arp 220 and Mrk 231 (Aladro et al. 2015). With the extreme starburst activity, we suggest that NGC 6240 also belongs to the HC₃N-poor galaxy, which is consistent with the result of Jiang et al. (2017) with non-detection of

Table 7. Detected lines in NGC 6240

Molecule	Frequency GHz	$\int T_{mb} dv$ (K km s ⁻¹)	v_{LSR} (km s ⁻¹)	FWHM (km s ⁻¹)	Column densities ($\times 10^{13}$ cm ⁻²)
CN ^a (1–0)	113.191	2.57 ± 0.13	7229.2 ± 11.4	468.1 ± 29.9	3665 ± 173
CN ^b (1–0)	113.491	4.50 ± 0.13	7206.9 ± 6.5	466.0 ± 16.1	...
*CO (1–0)	115.271	60.41 ± 0.42	7178.0 ± 1.3	403.8 ± 3.4	546166 ± 3797
C ₂ H (3–2)	262.067	4.28 ± 0.25	7144.0 ± 10.6	407.9 ± 30.6	130 ± 7.6
HC ₃ N (29–28)	263.792	0.28 ± 0.06	7174.7 ± 5.9	48.6 ± 11.6	11 ± 2.4
HCN (3–2)	265.886	9.22 ± 0.31	7207.7 ± 6.1	375.9 ± 14.5	7.8 ± 0.26
HCO ⁺ (3–2)	267.558	13.65 ± 0.66	7173.4 ± 9.4	397.4 ± 22.1	5.8 ± 0.28

The fluxes are in T_{mb} instead of T_A . For C₂H, the hyperfine transition, the flux integrated from 6799 km s⁻¹ to 7666 km s⁻¹. ^a is one of the groups for CN at 113.191GHz. ^b is the other group for CN at 113.491GHz. The asterisk * shows lines are optically thick and their column density would be underestimated. The column densities were calculated with the correction of an estimated source size.

Table 8. Detected lines in VII Zw 31

Molecule	Frequency GHz	$\int T_{mb} dv$ (K km s ⁻¹)	v_{LSR} (km s ⁻¹)	FWHM (km s ⁻¹)	Column densities ($\times 10^{13}$ cm ⁻²)
CN ^a (1–0)	113.191	0.30 ± 0.10	15472.7 ± 26.1	158.0 ± 57.0	129 ± 43
CN ^b (1–0)	113.491	0.75 ± 0.06	15415.1 ± 7.5	169.2 ± 14.0	...
*CO (1–0)	115.271	17.53 ± 0.06	15440.3 ± 0.3	182.7 ± 0.7	91210 ± 312
*CO (2–1)	230.538	41.81 ± 0.15	15442.6 ± 0.3	182.5 ± 0.7	...
C ₂ H (3–2)	262.067	0.47 ± 0.10	15449.0 ± 18.5	175.3 ± 39.5	884 ± 188
HC ₃ N (29–28)	263.792	$< 0.3(3\sigma)$...	178.2	< 7.46
HNCO (12 _{1,11} – 11 _{0,10})	264.694	0.47 ± 0.09	15538.9 ± 17.6	169.4 ± 33.7	82 ± 19
HCN (3–2)	265.886	1.26 ± 0.14	15440.3 ± 10.5	178.2 ± 20.1	0.66 ± 0.07
HCO ⁺ (3–2)	267.558	0.98 ± 0.15	15443.5 ± 15.2	198.6 ± 35.0	0.26 ± 0.04

The fluxes are in T_{mb} instead of T_A . For C₂H, the hyperfine transition, the flux integrated from 15250 km s⁻¹ to 15664 km s⁻¹. ^a is one of the groups for CN at 113.191GHz. ^b is the other group for CN at 113.491GHz. The asterisk * shows lines are optically thick and their column density would be underestimated. The column densities were calculated with the correction of an estimated source size.

Table 9. Column density ratios

Sources	$\frac{N_{H^{13}CN}}{N_{c-C_3H_2}}$	$\frac{N_{H^{13}CO^+}}{N_{c-C_3H_2}}$	$\frac{N_{HC_3N}}{N_{c-C_3H_2}}$
NGC 3079	< 0.26	< 0.08	< 0.65
NGC 4258	0.33 ± 0.11	0.12 ± 0.053	0.67 ± 0.30
NGC 6240
VII Zw 31
M 82	0.038 ± 0.0049	0.051 ± 0.0032	0.35 ± 0.10

Notes. The column densities of M 82 were obtained from the literature: [Aladro et al. \(2015\)](#). The upper limit ratios were calculated in NGC 3079 by only the blue-shift component of c-C₃H₂. The column density of blue-shift component of c-C₃H₂ is 2.0×10^{13} cm⁻².

HC₃N emission. The upper limit ratio of HC₃N/HCN in NGC 3079 is 0.03, which is consistent with [Lindberg et al. \(2011\)](#) as an HC₃N-poor galaxy. The non-detection HC₃N line in NGC 3079 and VII Zw 31 and $\frac{I(HC_3N)}{I(HCN)} < 0.15$ in NGC 4258 and NGC 6240, which implies that all four galaxies are HC₃N-poor galaxies.

5.5 Abundances of several molecules

In our sample, NGC 3079 and NGC 6240 host both AGN and powerful SB, while NGC 4258 is a pure AGN and VII Zw 31 is an ULIRG mainly powered by SB. C₂H, as a good PDR tracer, has similar abundances in NGC 3079, NGC 4258 and NGC 6240, which is an order of magnitude lower than that in VII Zw 31, indicating that strong UV fields in VII Zw 31 might be required for the enhancement of C₂H. c-C₃H₂ line is tentatively detected in NGC 3079 and NGC 4258. However, CN, whose abundance should also be enhanced in an X-ray chemistry ([Meijerink et al. 2007](#)), was not detected in NGC 4258. High resolution observations are needed to better understand CN and c-C₃H₂ emission in galaxies with AGN and/or starburst.

Column density ratios of molecules with less affect of opacity effects, were listed in Table 9. $\frac{N_{H^{13}CN}}{N_{c-C_3H_2}}$, $\frac{N_{H^{13}CO^+}}{N_{c-C_3H_2}}$ and $\frac{N_{HC_3N}}{N_{c-C_3H_2}}$ in NGC 3079, as non-detections, were lower than that in NGC 4258, which means that the abundances of H¹³CN, H¹³CO⁺, and HC₃N molecules are relatively lower in NGC 3079 than that in NGC 4258, if a fixed abundance of c-C₃H₂ is assumed in both galaxies. The ratios of $\frac{N_{H^{13}CO^+}}{N_{c-C_3H_2}}$,

$\frac{N_{H^{13}CN}}{N_{c-C_3H_2}}$ and $\frac{N_{HC_3N}}{N_{c-C_3H_2}}$ in NGC 4258 are higher than that in M 82 (Aladro et al. 2015), which may be caused by the enhancement of *c-C₃H₂* in M82 (Aladro et al. 2011).

6 SUMMARY AND CONCLUSIONS

We presented 3mm and 1mm band observations toward four nearby galaxies, including NGC 3079, NGC 4258, NGC 6240 and VII Zw 31, with the IRAM 30m telescope. The main results of this study are as follows.

1. We detected 10 molecular species in NGC 3079, 11 molecular species in NGC 4258, 6 molecular species in NGC 6240, and 6 molecular species in VII Zw 31, which expanded the molecular line data set for these galaxies. HC₃N 29-28 which requires high excitation condition, was detected in NGC 6240, and HNC 12-11 was detected for the first time in VII Zw 31. In addition, we tentatively detected the isotopic lines *H¹³CN* 1-0 and *H¹³CO⁺* 1-0 about 3σ level in NGC 4258. Optical depths of dense gas tracers were estimated as 4.1 for HCN 1-0 and 2.7 for HCO⁺ 1-0 in NGC 4258 with the detected *H¹³CN* 1-0 and *H¹³CO⁺* 1-0 lines.

2. We performed the detailed comparison of two nearby type II AGN: NGC 3079 and NGC 4258; and two gas-rich (U)LIRGs: VII Zw 31 and NGC 6240, with detected lines. Two groups of CN 1-0 in VII Zw 31 and NGC 6240, were detected and estimated as optically thin lines based on the line ratio. The high line ratio of HCO⁺/HCN 1-0 in NGC 4258 is inconsistent with typical value of pure AGNs and composite sources, while the line ratio of *H¹³CO⁺*/*H¹³CN* was close to unity, which is more relate to the relative abundances. The intensity ratio of HCO⁺/HCN lines might not be an ideal tool to identify AGN or starburst in galaxies. The ratio of ¹³CO/C¹⁸O 2-1 shows obvious difference in NGC 3079 and NGC 4258.

3. Under the LTE approximation, we derived column densities of various molecular species. With the relative abundances of C₂H, HNC, HCN, HCO⁺ and HNC normalized by CN, we found the environment of starburst in NGC 3079 might be similar to that in NGC 253. *c-C₃H₂* was detected, while CN were not detected, in NGC 4258. CN molecule shows abundance variations among different power sources of galaxies nuclei.

4. We find these four source are all HC₃N-poor galaxies. $\frac{I(HC_3N)}{I(HCN)} < 0.15$ in NGC 4258 and NGC 6240 and the non-detection HC₃N line in NGC 3079 and VII Z w 31.

ACKNOWLEDGEMENTS

We thank useful comments and suggestions from the anonymous referee. This work is supported by the National Key R&D Program of China (No. 2017YFA0402704), the Natural Science Foundation of China under grants of 11590783, the Youth Foundation of Hebei Province of China (No. A2011205067) and National Youth Fund (No. 11303008) and Astronomical Union Fund (No. U1831126). We thank the staffs at the IRAM 30m telescope for their kind help and support during our observations.

REFERENCES

- Aalto, S., Polatidis, A. G., Hüttemeister, S., & Curran, S. J. 2002, *A&A*, 381, 783
- Aladro, R., Martín-Pintado, J., Martín, S., Mauersberger, R., & Bayet, E. 2011, *A&A*, 525, A89
- Aladro, R., Martín, S., Martín-Pintado, J., et al. 2011, *A&A*, 535, A84
- Aladro, R., Viti, S., Bayet, E., et al. 2013, *A&A*, 549, A39
- Aladro, R., Martín, S., Riquelme, D., et al. 2015, *A&A*, 579, A101
- Braun, R., Oosterloo, T. A., Morganti, R., Klein, U., & Beck, R. 2007, *A&A*, 461,455
- Braine, J., Guelin, M., Dumke, M., et al. 1997, *A&A*, 326, 963
- Costagliola, F., Aalto, S., Rodriguez, M. I., et al. 2011, *A&A*, 528, A30
- Costagliola, F., Aalto, S., Sakamoto, K., et al. 2013, *A&A*, 556, A66
- Costagliola, F., Sakamoto, K., Muller, S., et al. 2015, *A&A*, 582, A91
- Cox, P., & Downes, D. 1996, *ApJ*, 473, 219
- Davis, T. A., Heiderman, A., Evans, N. J., & Iono, D. 2013, *MNRAS*, 436, 570
- Dickinson, D. F., Dinger, A. S. C., Kuiper, T. B. H., & RodriguezKuiper, E. N., 1980, *ApJ*, 237, L43
- Downes, D., & Solomon, P. M. 1998, *ApJ*, 507, 615
- Djorgovski, S., de Carvalho, R. R., & Thompson, D. J. 1990, *AJ*, 99, 1414
- Fairclough, J. H. 1986, *MNRAS*, 219, 1P
- Feruglio, C., Fiore, F., Piconcelli, E., et al. 2013, *A&A*, 558, A87
- Furuya, K., van Dishoeck, E. F., Aikawa, Y. 2016, *A&A*, 586, A127
- Greve, T. R., Papadopoulos, P. P., Gao, Y., & Radford, S. J. E. 2009, *ApJ*, 692, 1432
- Gao, Y., & Solomon, P. M. 2004, *ApJ*, 606, 271
- Gao, Y., & Solomon, P. M. 2004, *ApJS*, 152, 63
- García-Burillo, S., Martín-Pintado, J., Fuente, A., & Neri, R. 2000, *A&A*, 355, 499
- García-Burillo, S., Martín-Pintado, J., Fuente, A., & Neri, R. 2001, *ApJ*, 563, L27
- Graciá-Carpio, J., García-Burillo, S., Planesas, P., & Colina, L. 2006, *ApJ*, 640, L135
- Gerin, M., & Phillips, T. G. 2000, *ApJ*, 537, 644
- Goldsmith, Paul F., Young, Judith S. 1989, *ApJ*, 341, 718
- Goldsmith, P. F., & Langer, W. D. 1999, *ApJ*, 517, 209
- Herrnstein, J.R., Greenhill, L.J., Moran, J. M., Diamond, P. J., Inoue, M., Nakai, N., & Miyoshi, M. 1998, *ApJ*, 497, L69
- Heckman, T. M. 1980, *A&A*, 87, 152
- Henkel, C., Mauersberger, R., Wiklind, T., et al. 1993, *A&A*, 268, L17
- Henkel, C., Asiri, H., Ao, Y., et al. 2014, *A&A*, 565, A3
- Iono, D., Wilson, C. D., Takakuwa, S., et al. 2007, *ApJ*, 659, 283

- Imanishi, M., Nakanishi, K., Kuno, N., & Kohno, K. 2004, *AJ*, 128, 2037
- Imanishi, M., Nakanishi, K., Tamura, Y., Oi, N., & Kohno, K. 2007, *AJ*, 134, 2366
- Irwin, J. A., & Saikia, D. J. 2003, *MNRAS*, 344, 977
- Izumi, T., Kohno, K., Martín, S., et al. 2013, *PASJ*, 65, 100
- Izumi, T., Kohno, K., Aalto, S., et al. 2016, *ApJ*, 818, 42
- Leroy, A. K., Evans, A. S., Momjian, E., et al. 2011, *ApJ*, 739, L25
- Lepp, S., & Dalgarno, A. 1996, *A&A*, 306, L21
- Loenen, A. F., Spaans, M., Baan, W. A., & Meijerink, R. 2008, *A&A*, 488, L5
- Lindberg, J. E., Aalto, S., Costagliola, F., et al. 2011, *A&A*, 527, A150
- Lovas, F. J. 1992, *Journal of Physical and Chemical Reference Data*, 21, 181
- Jiang, X., Wang, J., & Gu, Q. 2011, *MNRAS*, 418, 1753
- Jiang, xuejian, Wang, junzhi, Gao, Y., et al. 2017, *A&A*,
- Jiménez-Vicente, J., Mediavilla, E., Castillo-Morales, A., & Bat-taner, E. 2010, *MNRAS*, 406, 181
- Juneau, S., Narayanan, D. T., Moustakas, J., et al. 2009, *ApJ*, 707, 1217-1232
- Kohno, K., Matsushita, S., Vila-Vilaró, B., et al. 2001, *The Central Kiloparsec of Starbursts and AGN: The La Palma Connection*, 249, 672
- Komossa, S., Burwitz, V., Hasinger, G., et al. 2003, *ApJ*, 582, L15
- Koda, J., Sofue, Y., Kohno, K., et al. 2002, *ApJ*, 573, 105
- Krause, M., Fendt, C., & Neiningner, N. 2007, *A&A*, 467, 1037
- Krips, M., Neri, R., García-Burillo, S., et al. 2008, *ApJ*, 677, 262-275
- Kulczak-Jastrzebska, M. 2017, *ApJ*, 835,121
- Martín, S., Krips, M., Martín-Pintado, J., et al. 2011, *A&A*, 527, A36
- Martín, S., Martín-Pintado, J., & Mauersberger, R. 2009, *ApJ*, 694, 610
- Martín, S., Mauersberger, R., Martín-Pintado, J., Henkel, C., & Garcia-Burillo, S. 2006b, *ApJS*, 164, 450
- Martín, S., Kohno, K., Izumi, T., et al. 2015, *A&A*, 573, A116
- Martín, S., Requena-Torres, M. A., Martín-Pintado, J., & Mauersberger, R. 2008, *ApJ*, 678, 245-254
- Meier, D. S., & Turner, J. L. 2012, *ApJ*, 755, 104
- Meijerink, R., & Spaans, M. 2005, *A&A*, 436, 397
- Meijerink, R., Spaans, M., & Israel, F. P. 2007, *A&A*, 461, 793
- Mills, E. A. C., Güsten, R., Requena-Torres, M. A., & Morris, M. R. 2013, *ApJ*, 779, 47
- Miyoshi, M., Moran, J. M., Herrnstein, J.R., Greenhill, L., Nakai, N., Diamond, P., & Inoue, M. 1995, *Nature*, 373, 127
- Müller, H. S. P., Schlöder, F., Stutzki, J., & Winnewisser, G. 2005, *Journal of Molecular Structure*, 742, 215
- Nakajima, T., Takano, S., Kohno, K., & Inoue, H. 2011, *ApJ*, 728, L38
- Neill, J. L., Wang, S., Bergin, E. A., et al. 2013, *ApJ*, 770, 142
- Nguyen, Q. -R., Jackson, J. M., Henkel, C., Truong, B., Mauersberger, R. 1992, *ApJ*, 399, 521
- Omout, A. 2007, *Reports on Progress in Physics*, 70, 1099
- Ogle, P. M., Lanz, L., & Appleton, P. N. 2014, *ApJ*, 788, L33
- Papadopoulos, P. P. 2007, *ApJ*, 656, 792
- Paglione, T. A. D., Wall, W. F., Young, J. S. et al. 2001, *ApJ*, 135, 183
- Pérez-Beaupuits, J. P., Aalto, S., & Gerebro, H. 2007, *A&A*, 476, 177
- Pickett, H. M., Poynter, R. L., Cohen, E. A., et al. 1998, *J. Quant. Spectrosc. Radiative Transfer*, 60, 883
- Privon, G. C., Herrero-Illana, R., Evans, A. S., et al. 2015, *ApJ*, 814, 39
- Privon, G. C., Aalto, S., Falstad, N., et al. 2017, *ApJ*, 835, 213
- Radford, S. J. E., Downes, D., & Solomon, P. M. 1991, *ApJ*, 368, L15
- Rodriguez-Franco, A., Martín-Pintado, J., & Fuente, A. 1998, *A&A*, 329, 1097
- Sage, L. J., & Solomon, P. M. 1987, *ApJ*, 321, L103
- Sanders, D. B., & Mirabel, I. F., 1996, *ARA&A*, 34, 794
- Sawada-Satoh, S., Ho, P. T. P., Muller, S., Matsushita, S., & Lim, J. 2007, *ApJ*, 658, 851
- Solomon, P. M., Sanders, D. B., & Scoville, N. Z. 1979, *The Large-Scale Characteristics of the Galaxy*, 84, 35
- Scoville, N. Z., Sanders, D. B., Sargent, A. I., Soifer, B. T., & Tinney, C. G. 1989, *ApJ*, 345, L25
- Scoville, N., Sheth, K., Walter, F., et al. 2015, *ApJ*, 800, 70
- Sage, L. J., Solomon, P. M. 1987, *ApJ*, 321, 103
- Snell, R. L., Narayanan, G., Yun, M. S., et al. 2011, *AJ*, 141, 38
- Sofue, Y., & Irwin, J. A. 1992, *ApJS*, 44, 353
- Sosa-Brito, R. M., Tacconi-Garman, L. E., Lehnert, M. D., & Gallimore, J. F. 2001, *ApJS*, 136, 61
- Schweizer, F. 2005, *ASSL*, 329, 143
- Sutton, E. C., Blake, G. A., Masson, C. R., & Phillips, T. G. 1985, *ApJS*, 58, 341
- Radford, S. J. E., Downes, D., & Solomon, P. M. 1991, *ApJ*, 368, L15
- Tacconi, L. J., Genzel, R., Tecza, M., et al. 1999, *ApJ*, 524, 732
- Tsai, M., & Hwang, C.-Y. 2015, *VizieR Online Data Catalog*, 515,
- Tinney, C. G., Scoville, N. Z., & Soifer, B. T. 1990, *ApJ*, 362, 473
- van Dishoeck, E. F., & Blake, G. A. 1998, *ARA&A*, 36, 317
- Walter, F., Bolatto, A. D., Leroy, A. K., et al. 2017, *ApJ*, 835, 265
- Wang, J., Zhang, Z., Shi, Y. 2011, *MNRAS*, 416, L21
- Wang, J., Zhang, J., Shi, Y., & Zhang, Z. 2013, *ApJ*, 778, L39
- Wang, J., Zhang, Z.-Y., Qiu, J., et al. 2014, *ApJ*, 796, 57
- Wang, J., Zhang, Z.-Y., Zhang, J., Shi, Y., & Fang, M. 2016, *MNRAS*, 455, 3986
- Wilson, C. D., Petitpas, G. R., Iono, D., et al. 2008, *ApJS*, 178, 189-224
- Wooten, A., 1981, *ApJ*, 245, 105
- Yuan, F., Markoff, S., Falcke, H., & Biermann, P. L. 2002, *A&A*, 391,139-148
- Zhang, J. S., Henkel, C., Guo, Q., & Wang, J. 2012, *A&A*, 538, A152

APPENDIX A: MOLECULAR SPECIES IN THESE SOURCES

This paper has been typeset from a $\text{\TeX}/\text{\LaTeX}$ file prepared by the author.

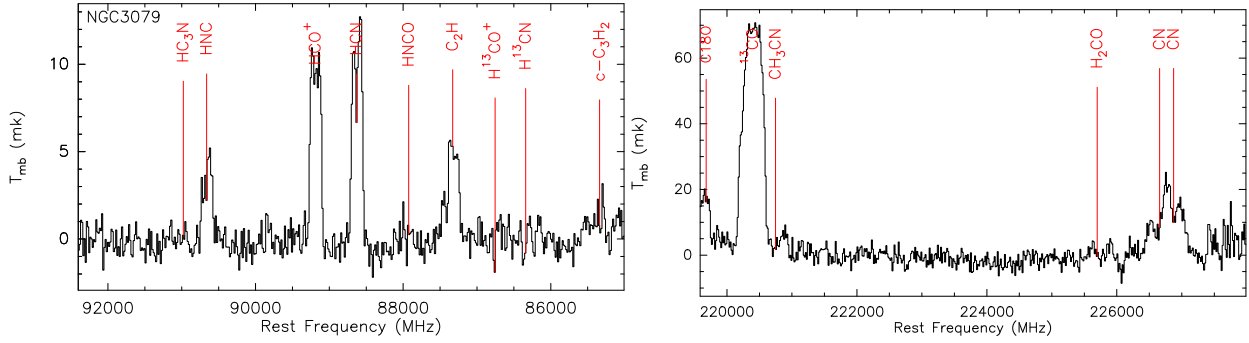


Figure A1. Molecular species of NGC 3079, Left: band ranges from 85 GHz-92 GHz, with RMS of 1.13 mK at the velocity resolution of 54.67 km s^{-1} . Right: band ranges from 220 GHz-227 GHz, with RMS of 3.29 mK at the velocity resolution of 21.42 km s^{-1} .

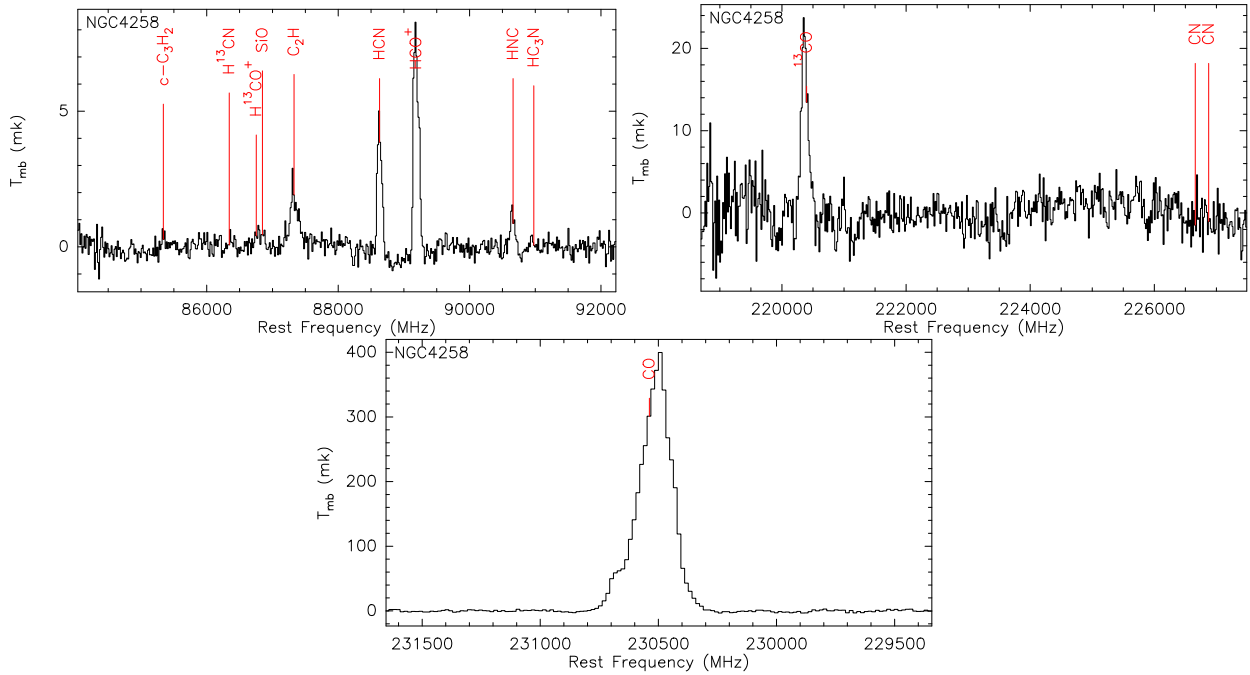


Figure A2. Molecular species of NGC 4258. Top left: band ranges from 85 GHz-91 GHz, with the RMS of 0.33 mK at the velocity resolution of 54.67 km s^{-1} . Top right: band ranges from 219 GHz-227 GHz, with the RMS of 2.33 mK at the velocity resolution of 21.36 km s^{-1} . Bottom: band ranges from 229 GHz-236 GHz, with RMS of 1.25 mK at the velocity resolution of 20.57 km s^{-1} .

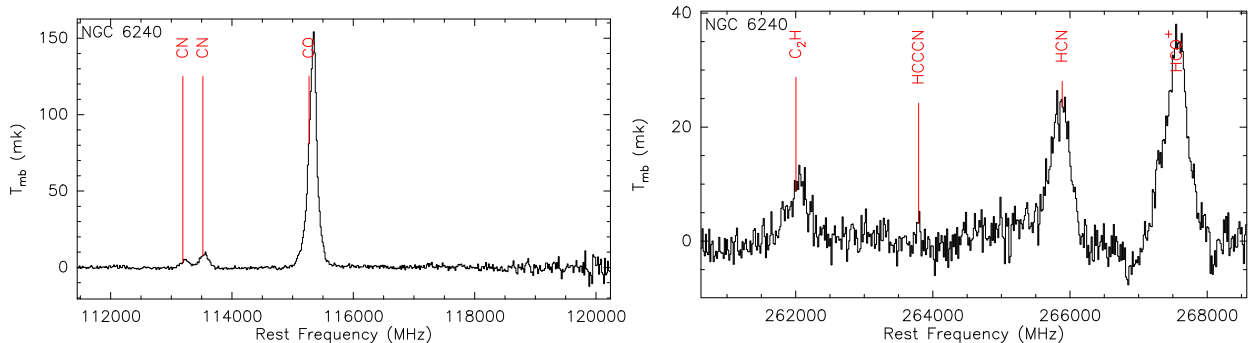


Figure A3. Molecular species of the NGC 6240. Left: band ranges from 109 GHz-117 GHz, with RMS of 2.03 mK at the velocity resolution of 41.53 km s^{-1} . Right: band ranges from 255 GHz-262 GHz, with RMS of 2.40 mK at the velocity resolution of 18.25 km s^{-1} .

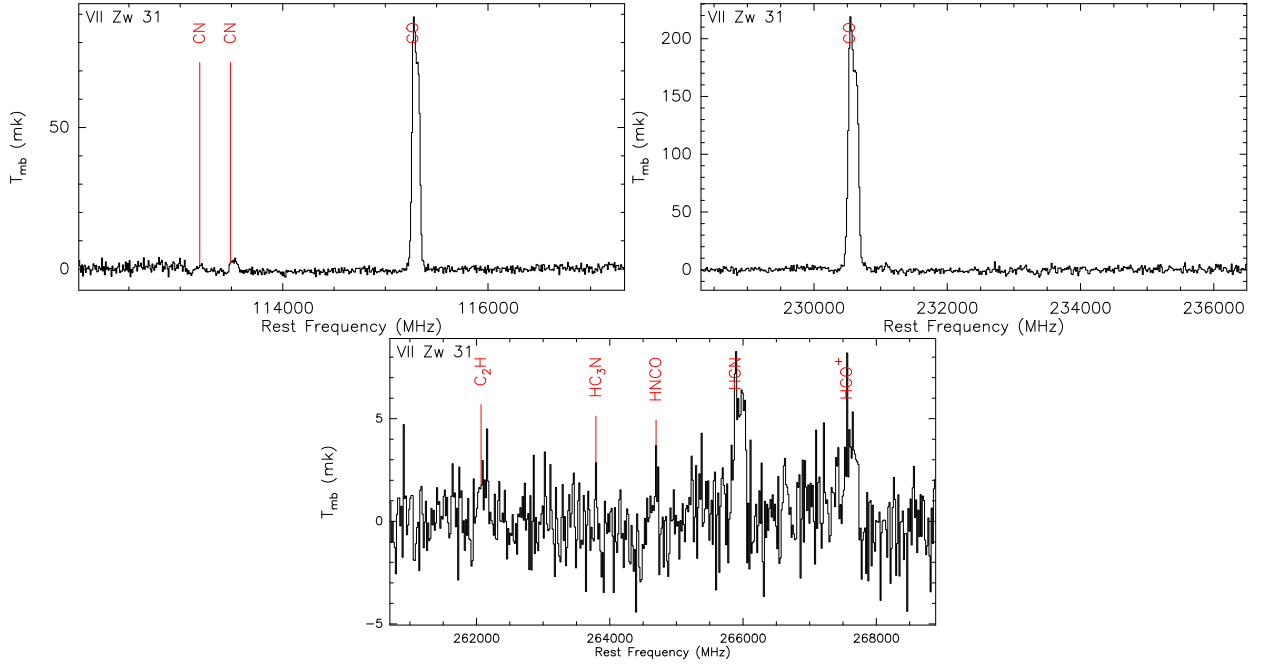


Figure A4. Molecular species of the VII Zw 31. Left: band ranges from 108 GHz-111 GHz, with RMS of 1.15 mK at the velocity resolution of -23.48 km s^{-1} . Middle: band ranges from 217 GHz-224 GHz, with RMS of 2.08 mK at the velocity resolution of 21.68 km s^{-1} . Right: band ranges from 248 GHz-255 GHz, with RMS of 1.59 mK at the velocity resolution of 18.77 km s^{-1} .